Science of Sintering, **51** (2019) 39-56

doi: https://doi.org/10.2298/SOS1901039T

UDK 692.533.1; 676.017.2; 665.7.035.8

Thermal and Mechanical Behavior of Composite Mortars Containing Natural Sorptive Clays and Fly Ash

Anja Terzić[1*)], Lato Pezo[2], Ljiljana Miličić[1], Nevenka Mijatović[1], Zagorka Radojević[1], Dragan Radulović[3], Ljubiša Andrić[3]

[1]Institute for Materials Testing IMS, Vojvode Mišića Bl. 43, 11000 Belgrade, Serbia

[2]Institute of General and Physical Chemistry, University of Belgrade, Studentski Trg 12-16, 11000 Belgrade, Serbia

[3]Institute for Technology of Nuclear and other Mineral Raw Materials, Franchet d'Esperey 86, 11000 Belgrade, Serbia

Abstract:

Mineral additives are extensively applied as cement replacement materials in both construction concrete and mortar. Fly ash is one of the most commonly utilized additives which improve rheological properties, as well as thermal and mechanical behavior of mortar, and as such it has been widely investigated. This industrial byproduct comprises heavy metals in its composition; therefore further research is needed to optimize its effective dosage. Moreover, certain sorptive clays, such as natural zeolite and bentonite, can prevent migration of toxic elements from fly ash by immobilizing them in their structure. Ten experimental mortars are prepared with Portland cement, river sand and addition of fly ash, zeolite and/or bentonite in accordance with chemometric experimental design rules. The aim of the study was to investigate the effect of mineral additives on thermal and mechanical performances of mortar. Thermal characteristics were monitored via dilatometric analysis and DTA method. Principal component analysis was used on the results of physico-mechanical testing (workability, bulk density, water absorption, shrinkage, compressive and flexural strength) to enable the divisions of the observed samples into groups in the factor space. The performance of Artificial Neural Network was compared with the experimental data in order to develop rapid and accurate method for prediction of mechanical parameters of mortar. The ANN model showed high overall prediction accuracy (r^2 = 0.989, during training cycle). The test results indicate that incorporation of the mineral additives gave cost effective mortars with sufficiently good properties. However, tools of analytical modeling highlighted mortar with zeolite and fly ash as the optimal composition regarding its mechanical performance.

Keywords *Dilatometry, DTA; Analytical modeling; SEM; Construction composites.*

1. Introduction

With concrete and mortar being the most prevailing construction materials, the manufacturing of cement still represents a huge pollution risk. Production rate of Portland cement is set at approximately 3000 Mt/year [1, 2]. The fabrication of cementitious composites also induces consumption of natural resources and leads to their severe depletion [3]. Current innovations in this industrial sector are aiming towards either full or partial

*) **Corresponding author:** anja.terzic@institutims.rs

replacing of the cement in non-shaped building materials with other pozzolana [4-7]. Available resource utilized as mineral additive is a practical solution for the reduction material's cost, although it can also be a means for performances improvement [8-12]. The employment of coal combustion byproducts (fly, bottom, and landfill ash) in the building industry is a common practice which is in accordance with the environmental requirements [13-15]. In contemporary building industry, fly ash is a standard low-cost binder with characteristics (pozzolanic behavior, high reactivity) matching to those of Portland cement [16, 17]. However, this raw material contains hazardous substances such as heavy metals. Even though their content is below upper limit [13], non-degradable heavy metals tend to accumulate, upon being leached, and thereby impose a severe threat to the environment [18-20]. Inhibition of leaching mechanisms and of heavy metals isolation within composite's microstructure is accomplished by employment of a component with sorption ability [21, 22].

Heavy metal ions are partially immobilized in cement hydrates, but the application of clayey raw materials (natural zeolite and bentonite) characterized by hydrophilicity and sorptivity significantly enhances fixation mechanisms [22]. The replacement of weakly bonded cations with other cations takes place on surfaces or within clay's structural cavities [28-30]. These molecular sieves are letting through molecules of certain size, while molecules of adsorbed substances are dissipating in the cavities of dehydrated clay [23]. Zeolite is a 3D crystalline framework of SiO_4 and AlO_4 tetrahedra linked by O atoms [23, 25], while bentonite is composed of two SiO_4 tetrahedra and octahedral sheet of AlO_4 ions [24]. Zeolite honeycomb structure with channels of molecular dimensions (3-10 Å) absorbs and loses water up to 30 % of its weight thus enabling ion-exchange chemistry and reception of Na^+, K^+, Mg^{2+}, Ba^{2+}, Ca^{2+} cations, transition metal ions, molecules or ion groups (NH_3, CO_3^{2-}, NO_3^-) [26-28]. In bentonite's 2:1 layer structure, Van Der Waals forces tie the piled layers of basic units simplifying the ion exchange within interlayer space [29-30]. Properties like large specific surface area, uniform porosity, good thermal stability and pozzolanic activity are advantageous for application of the clays in binders, concretes, mortars and non-autoclaved silicate products [1, 2, 22, 23]. Improvement of mechanical performances in cementitious materials is enabled by presence of additional pozzolana (calcium silicates and calcium aluminosilicates) formed in reactions between SiO_2 and Al_2O_3 from clays with $Ca(OH)_2$ [23]. Therefore, zeolite and bentonite not only immobilize heavy metals, their application also leads to acceleration of cement hydration, increase in early strengths, decrease in bulk density (lighter structures), evener surfaces, better drying mechanism, reduction in various processes (chloride penetration, sulfate attack, expansion due to alkali silica reaction), decrease in autogenous deformation and micro-cracking [2, 22, 23, 31].

The effects of the application of three mineral additives (zeolite, bentonite, and fly ash) on the properties of mortar were studied. The clayey materials were used as sorbents to immobilize leaching of heavy metals from fly ash. The thermal, microstructural and mechanical properties of ten composite mortars were investigated. Artificial Neural Networks (ANN) was employed in mathematical modeling of physico-mechanical behavior of mortars. ANN are a good modeling tool since they provide the empirical solution to the problems from a set of experimental data, and are capable of handling complex systems with non-linearities and interactions between decision variables [33-37]. The aim of the investigation was to incorporate industrial byproduct and sorptive clays in the design of mortars, thereby offering a new solution for novel ecological material with advanced performances.

2. Experimental Procedures

2.1. Raw materials

Experimental mortar samples were prepared from cement and sand aggregate as base

resources. Fly ash and clays were used in different ratios as mineral additives. Standard Portland cement CEM I 42.5R (Lafarge), with 97.5 % of particles in range 0.0 - 0.63 mm and 292 m^2/kg specific surface area, was used as binder. SiO_2 (22 %) and CaO (62 %) were predominant oxides in the cement composition. Utilized fly ash, collected directly from the filter of "Kolubara" power-plant (Serbia), is a byproduct of lignite coal combustion. The specific surface area of ash was 283 m^2/kg. The diameters of ash particles varied from 1.9 μm to 1258 μm. The applied ash is an aluminosilicate containing 63 % of SiO_2 and 18 % of Al_2O_3. The sorptive clays are also aluminosilicates. Bentonite (Šipovo deposit, Bosnia & Herzegovina) has montmorillonite content as high as 70 %. The silicon oxide content was 60 %, while aluminium oxide participated with 13 % in the chemical composition. Bentonite was pulverized in an agate stone mill (KHD Humboldt Wedag) prior to the experimental work. Thus acquired specific surface area was 79.1 m^2/kg. The size of particles spanned in the range -37+75 μm. Zeolite clay, which comprised zeolitizated volcanic ash and small amounts of quartz, plagioclase and biotite, was issued from Vranjska banja deposit (Serbia). Two main oxides - SiO_2 and Al_2O_3 participated with 65 % and 12 % in the zeolite composition, respectively. The specific surface area of pulverized zeolite was 75.5 m^2/kg (diameter of particles: -37+300 μm). River sand was applied as aggregate in the mortar's mix design. Bulk density of the aggregate was 1720 kg/m^3 in loose condition and 1980 kg/m^3 in pressed condition. With SiO_2 content as high as 97.57 %, aggregate primarily contained quartz, less abundant feldspar and very small traces of mica.

2.2. Experimental design

Eleven mortar mixtures were prepared. The S_0 sample was a standard cement mortar, which was used for the comparison with other composites (S_{1-10}). The ratios of the raw materials were chosen in accordance with the rules of chemometric experimental design. Experimental data for the analysis were derived using the Simplex-lattice design, with 3 levels and 3 parameters (10 mixtures and 1 control). The selected mix design is shown in Tab. I.

Tab. I The mix design of the experimental mortars.

Sample	S_0	S_1	S_2	S_3	S_4	S_5	S_6	S_7	S_8	S_9	S_{10}
Cement, %	25	17.5	17.5	17.5	17.5	17.5	17.5	17.5	17.5	17.5	17.5
Aggregate,%	75.0	75.0	75.0	75.0	75.0	75.0	75.0	75.0	75.0	75.0	75.0
Fly ash, %	-	7.5	-	-	5.0	2.5	5.0	2.5	2.5	-	-
Zeolite, %	-	-	7.5	-	2.5	5.0	-	-	2.5	2.5	5.0
Bentonite, %	-	-	-	7.5	-	-	2.5	5.0	2.5	5.0	2.5

The mortar samples were prepared according to the standard procedure (SRPS EN 480-1:2015). The aspect ratio between binder and aggregate was 1:3 in all composites. Mineral additives were employed in total quantity of 30 % (calculated from the mass of binder), with respect to EN 197-1. The aggregate comprised three fractions of river sand (-0.2+0.6; -0.6+1.0; and -1.0+2.0 mm) in 1:1:1 ratio. The water to cement ratio was fixed at 0.5 for all mixes. The dry mixes were homogenized by a Controls (Italy) laboratory mixer. The water was added during mixing procedure. The green mixes were cast in steel molds (40×40×160 mm) and preserved in a chamber with 90±5 % humidity and 20±2 ^oC for 24^h. On the second day, the samples were removed from molds and stored under the same conditions for next 6 days, after which they were cured at 20±2 ^oC and 60±5 % humidity.

Rheology of green mortar, i.e. workability of green mixture (W, in mm) was estimated via slump test using a flow table (ASTM C230). Bulk density (BD, in kg/m^3) was calculated as a quotient of mortar sample mass and its volume. Shrinkage of mortar was estimated from the hydration and hydraulic dimensional changes measured on the samples

(during 28 days) according to the following formula:

$$SH = \frac{\Delta l}{l_0} (\text{mm/m}) \qquad (1)$$

where: l_0 is initial dimension of the sample (16 cm) and Δl is difference between initial dimension and dimension measured at exact period of time (1st, 4th, 7th, 14th, 21st and 28th day since the start of the experiment).

Water absorption (WA, in %) was determined from the weight difference between dry and water-saturated samples previously immersed in boiling water for 2 hours. The flexural (FS, in MPa) and compressive (CS, in MPa) strengths of hardened mortar were tested on an Amsler laboratory hydraulic press, in accordance with the SRPS EN 1015-11:2008/A1:2008. Tests for compressive strength were conducted on halves of experimental prisms (40×40 mm cross-sectional area). Testing was conducted on the 1st, 4th, 7th, 14th, 21st and 28th day since the start of the experiment.

2.3 Instrumental analyses

The chemical composition of mortars was analyzed via X-ray fluorescence method on an ED 2000 XRF spectrophotometer (Oxford Instruments, UK). The representative samples (100 g) were pulverized in a laboratory vibratory mill (HSM, Herzog, Germany) prior to the testing (Standard: SRPS EN196-2:2015). Averaged values are given in Tab. II. The loss on ignition (LoI) was determined as a weight difference between 20 °C and 1000 °C.

Tab. II Chemical composition of the mortars.

Oxide,%	**S_0**	**S_1**	**S_2**	**S_3**	**S_4**	**S_5**	**S_6**	**S_7**	**S_8**	**S_9**	**S_{10}**
SiO_2	75.89	74.92	75.91	73.25	74.88	75.7	73.99	72.94	75.59	76.56	73.21
Al_2O_3	1.96	2.95	2.72	2.49	3.11	2.95	2.82	2.92	2.31	1.79	3.56
Fe_2O_3	0.75	1.51	0.21	0.98	1.69	0.03	1.67	0.51	0.35	0.1	0.63
CaO	13.86	12.38	12.95	15.04	12.92	13.55	12.47	15.41	14.52	13.95	14.62
MgO	0.17	0.17	0.09	0.07	0.21	0.09	0.06	0.05	0.09	0.1	0.08
K_2O	0. 09	0.07	0.08	0.05	0.07	0.07	0.07	0.04	0.05	0.08	0.02
Na_2O	0.03	0.02	0.04	0.02	0.02	0.03	0.03	0.01	0.04	0.03	0.05
TiO_2	0	0.02	0.01	0.06	0.01	0.01	0.05	0.06	0.03	0.01	0.05
LoI	7.34	7.96	7.99	8.04	7.09	7.57	8.84	8.06	7.02	7.38	7.78

Dilatometry was conducted on a SETSYS TMA analyzer (25-1000 °C; 10 °C/min). Approximately 25 mg of pulverized mortar was compacted into a tablet (∅ =5.0 mm). After placing the tablet in to a corundum crucible, it was pressed by a ram with a load of 0.01 N. The shrinkage (S_d, in %) was calculated as a quotient of the sample's initial height (h_0) and difference between initial height and height measured at a specific temperature (h_i), Eq (2):

$$S_d = \frac{h_0 - h_i}{h_0} \cdot 100\% \qquad (2)$$

A differential thermal (DTA) analysis was conducted in the temperature range 25-1000 °C in an alumina pan at a constant heating rate of 10 °C/min and static air flow (SETSYS TG-DTA/DSC, SETARAM Instrumentation).

The morphology of the crushed mortar samples was characterized by scanning electron microscopy (JEOL JSM-IT300). The samples were covered with gold using a sputter

machine, type BALTEC-SCD-005, for improvement of the conductivity prior to the imaging.

2.4. Statistical analysis and mathematical modeling

Response surface methodology (RSM) was employed to describe the effects of the test variables on the observed responses and to determine test variables interrelationships. The evaluation of RSM and ANOVA of the obtained results was performed using Statistica software version 10 (StatSoft Inc. 2010, USA)®.

Principal Component Analysis (PCA) was used as a central mathematical tool in exploratory data analysis. This multivariate technique transforms the data are into orthogonal components that are linear combinations of the original variables. The procedure is performed by Eigenvalue decomposition of a data correlation matrix [38]. Thereby, the first component has the largest possible variance. The maximum separation among clusters of parameters is acquired by this analysis. Also, a considerable reduction in a number of variables and the detection of structure in the relationship between measuring parameters is enabled. The full auto scaled data matrix consisting of different mixtures was submitted to the PCA, which resulted is spatial relationship between processing parameters and formed graphic differentiation between observed samples.

Artificial Neural Network model (ANN) was used to predict the values of the experimental data, i.e. tested properties (W, SH, WA, BD, CS, FS). The database for ANN was randomly divided into: training data (60 %), cross-validation (20 %) and testing data (20 %). The cross-validation data set was used to test the performance of the network, while training was in progress as an indicator of the level of generalization and the time at which the network has begun to over-train. The testing data set was used to examine the network generalization capability. To improve the behavior of the ANN, both input and output data were normalized. In order to obtain good network behavior, it is necessary to make a trial and error procedure and also to choose the number of hidden layers, and the number of neurons in hidden layer(s). A multi-layer perceptron model (MLP) consisted of three layers (input, hidden and output). Such a model has been proven as a quite capable of approximating nonlinear functions [39] giving the reason for choosing it in this study. In this work the number of hidden neurons for optimal network was ten. Broyden-Fletcher-Goldfarb-Shanno (BFGS) algorithm was used for ANN modeling. After defining the architecture of ANN, the training step was initiated. The training process was repeated several times in order to get the best performance of the ANN, due to a high degree of variability of parameters. It was accepted that the successful training was achieved when learning and cross-validation curves (Sum of Squares vs. training cycles) approached zero. Testing was carried out with the best weights stored during the training step. Coefficient of determination (r^2) and SOS were used as parameters to check the performance (i.e. the accuracy) of the obtained ANN.

Sensitivity analysis is employed in studying the effects of observed input variables, uncertainties in the obtained models and general network behavior. Neural networks were tested using sensitivity analysis, to determine whether and under what circumstances obtained model might result in an ill-conditioned system [39]. On the basis of the developed ANN model, sensitivity analysis was performed in order to more precisely define the influence of processing variables on the observed outputs. The infinitesimal amount (+0.0001 %) has been added to each input variable, in 10 equally spaced individual points encompassed by the min and max the training data. These signals were normally distributed with a constant intensity and frequency. It was used to test the model sensitivity and measurement errors.

The accuracy of the models, i.e the numerical verification of the developed models was tested using coefficient of determination (r^2), reduced chi-square (χ^2), mean bias error (MBE), root mean square error (RMSE) and mean percentage error (MPE). These commonly used parameters can be calculated as follows [40, 41].

$$\chi^2 = \frac{\sum_{i=1}^{N}(x_{\exp,i} - x_{pre,i})^2}{N-n},\ RMSE = \left[\frac{1}{N}\cdot\sum_{i=1}^{N}(x_{pre,i} - x_{\exp,i})^2\right]^{1/2},$$
$$MBE = \frac{1}{N}\cdot\sum_{i=1}^{N}(x_{pre,i} - x_{\exp,i}),\ MPE = \frac{100}{N}\cdot\sum_{i=1}^{N}\left(\frac{\left|x_{pre,i} - x_{\exp,i}\right|}{x_{\exp,i}}\right) \quad (3)$$

Where $x_{exp,i}$ stand for the experimental values and $x_{pre,i}$ are the predicted values by calculating from the model for these measurements. N and n are the number of observations and constants, respectively.

3. Results and Discussion

According to X-ray fluorescence analysis (Tab. II), the chemical composition of $S_{1\text{-}10}$ experimental mortars did not significantly differ from the cement mortar (S_0). SiO_2, as the most abundant oxide, varied from 72.94 % detected in S_7 sample to the maximum of 76.56 % in S_{10}. Cement mortar comprised silicon oxide in the quantity of 75.89 %. Similar ratio was observed for the other oxides, as Al_2O_3 ranged from 1.79 % (S_9) to 3.11 % (S_4), and CaO from the lowest 12.38 % noticed in S_1 to the maximal CaO 15.41 % in S_7. Fe_2O_3, MgO, K_2O, Na_2O, and TiO_2 can be considered minorly present oxides because their individual contents were less than 1 %. CaO in the mortar composition, as well as certain percentage of Fe_2O_3 and MgO, originated from Portland cement. Zeolite and fly ash additions induced the increase in SiO_2, Al_2O_3, Na_2O and K_2O content. Bentonite has a high percentage of SiO_2 , but in total composition the addition of bentonite mostly influenced the increase in TiO_2 content and elevated the loss on ignition. SiO_2, mineralogically present as quartz in mortars, primarily originated from the sand aggregate. A characteristic mineral-phase composition for cement mortar upon fully conducted hydration comprises alite (Ca_3SiO_5); belite (β-Ca_2SiO_4), portlandite ($Ca(OH)_2$), and calcite ($CaCO_3$) as the most abundant minerals. These phases are accompanied by lesser amounts of brownmillerite (Ca_2FeAlO_5) and tricalcium aluminate ($Ca_3Al_2O_6$) [42]. The addition of fly ash, characterized as aluminosilicate, does not significantly alter mortar's mineralogical composition, although it contributes with certain amount of quartz mineral phase [13]. Zeolite brings about presence of tecto-silicate minerals, usually heulandite –a hydrous calcium and aluminium silicate, $(Ca,Na)_{2\text{-}3}Al_3(Al,Si)_2Si_{13}O_{36}\cdot 12H_2O$) [40]. Analogously, the bentonite addition led to the appearance of smectite in the phase composition of a mortar. This mineral is usually phyllosilicate montmorillonite with 2:1 layer distribution, $(Na,Ca)_{0.33}(Al,Mg)_2(Si_4O_{10})(OH)_2\cdot nH_2O$) [41].

3.1. Thermal behavior of the experimental mortars

Thermal behavior of experimental mortars was assessed by means of differential thermal analysis and dilatometry.

Hydration mechanisms and thermal reactions that took place upon heating up to 1200 ^oC were observed on two mortar samples: S_4 – mortar with addition of fly ash and zeolite and S_6 – mortar with addition of fly ash and bentonite. The obtained results were compared with the DTA curve of standard cement mortar (S_0), and illustrated in Fig. 1a.

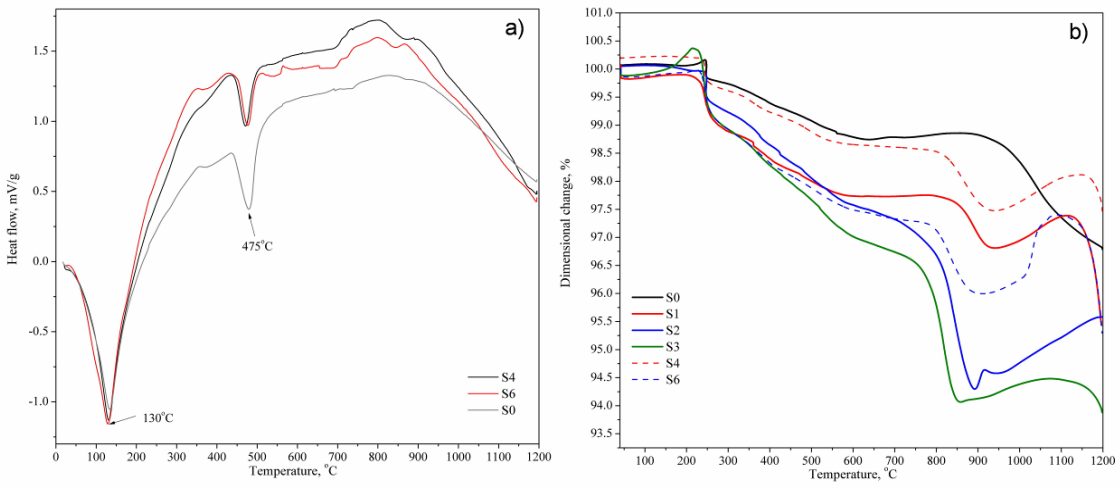

Fig. 1. Thermal behavior of mortars: a) differential thermal analysis; b) dilatometry.

DTA curves of composite mortars S_4 and S_6 formed two prominent peaks fully corresponding to those recorded on the sample of cement mortar (S_0). The initial effects were registered in the vicinity of 130 °C; namely 129.03 °C and 131.60 °C for S_6 and S_4, respectively. The first protruding effect in the cement mortar (S_0) was located at moderately higher temperature: 133.72 °C. The intensities of the well defined endothermic maxima, characteristic for the S_4 and S_6 samples, were approximately equal. The effect registered in S_0 mortar was less acute. The dehydration of $AH_3 \cdot H_2O$ gel is normally associated with endothermic reactions that take place at approximately 120 °C [43]. The exact temperature of dehydration depends on the type of cement and presence of mineral additives. The initial peak in cement mortar (S_0) appeared at 133.72 °C, while the peaks characteristic for fly-ash-and-zeolite and fly-ash-and-bentonite mortars were observed at lower temperatures meaning that all mineral additions acted as pozzolana and accelerated cement hydration. The development of ettringite and colloidal C-S-H gel in the interval 100 - 150 °C contributes to the intensity of the first peak in all observed mortars [44]. The additions of zeolite and bentonite intensified the observed reactions at 130 °C. Zeolite, i.e. its mineral heulandite, exhibits a notable endothermic effect at 120 °C as a result of single-step dehydration [40]. Similarly, bentonite main mineral - montmorillonite dehydrates at approximately 100 °C [41]. The hydration water comprised in the bentonite structure is further removed through a sequence of thermal reactions in the 100 - 450 °C interval (small exothermal peak at 350 °C, endothermic valley 350 - 440 °C).

The second significant effect was observed in the vicinity of 475 °C. The present peaks are endothermic with maxima located at 479.29 °C (S_0), 471.05°C (S_4) and 476.96 °C (S_6). These reactions can be associated with the decomposition of $C_{12}A_7$ aluminate phase in Portland cement. The dehydration of calcium aluminate and alumina hydrates is near finalization at 500 °C. The exact temperature depends on mineral additives. The reaction is usually marked by an endothermic peak on cement's DTA curve [45]. The addition of fly ash and zeolite, i.e. fly ash and bentonite, has moderately accelerated mentioned reaction mechanism. The changes are marked by shifting of maximum of at 475 °C peak to a lower temperature in both S_4 and S_6 diagrams.

Upon second endothermic effect, all three curves (S_0, S_4 and S_6) proceeded into a continuous complex exothermic hump (550 - 950 °C). The hump of each sample consists of several small endothermic and exothermic peaks. The maximum for the cement mortar was registered at 830.72 °C. S_4 sample showed an exothermic effect at 853.41 °C, followed by two smaller endothermic peaks at 711.20 and 907.05 °C. The peaks located above 700 °C

correspond to the rearrangements in the heulandite crystalline structure, since zeolite minerals are thermally stable up to 700 - 800 °C [40]. The DTA curve of S_6 mortar has a series of infinitesimal effects located on the exothermic hump. The most significant is the exothermic effect at 824.50 °C. This peak is followed by another exothermic effect at 902.3 °C. In bentonite, montmorillonite structure is preserved up to 850 °C, only to swiftly decompose during the following 50 °C [41]. The peak at 824 °C marks the start of montmorillonite decomposition in the S_6 sample. Since all samples (S_0, S_4, S_6) comprised quartz due to the application of river sand as aggregate, the effects located above 500°C might correspond to the polymorphic transformation of α- into β-quartz (at 573 °C) [43]. The effects in the vicinity of 800 - 900 °C correspond to the calcination, i.e. decomposition of calcite into CaO and CO_2. $CaCO_3$ was present in low abundance; thereby the reactions were not intense. The final step in the decomposition of calcium aluminate phases is expected to take place at 950 °C which is marked by endothermic streaming of DTA curves. The formation of molten phase in the cementitious systems did not appear during observed thermal interval (25 - 1200 °C). DTA curves recorded for cement mortar and composite mortars were similar, with one main difference - the intensity of the exothermic hump. Namely, energy liberated during thermal treatment of mortar with fly ash and zeolite addition (S_4) was higher than that of S_6 mortar with ash and bentonite as additions, as well as cement mortar. Therefore, the applied mineral additions bring about changes in cement hydration, which consequently leads to the alternations in physico-mechanical properties of mortars.

Dilatometric analysis was conducted on composite mortars and cement mortar, and the obtained results are illustrated in the Fig. 1b. The results of actually dimensional changes that took place during heating from ambient temperature up to 1200°C are condensed and displayed in Tab. III.

Tab. III Dimensional changes of mortars $S_{0\text{-}10}$ registered during thermal treatment in dilatometer.

Temperature	25-230°C	230-630°C	630-900°C	900-1200°C		
	Dimensional change, %					∑, %
S_0	-0.25*	1.5	-0.1	2.0		3.15
Temperature	25-230°C	230-800°C	800-900°C	900-1100°C	1100-1200°C	
	Dimensional change, %					∑, %
S_1	-0.1	2.1	1.0	-0.7	1.9	4.2
S_2	0.1	3.0	2.8	-1.3		4.6
S_3	-0.2	3.9	2.0	-0.3	0.4	5.8
S_4	0	2.0	1.0	-0.7	0.7	3.0
S_5	-0.1	2.7	1.5	-0.9		3.2
S_6	-0.1	2.7	1.3	-1.5	2.1	4.5
S_7	-0.1	2.5	2.0	-0.5	0.7	4.6
S_8	-0.1	3.0	2.3	-0.5	0.6	5.3
S_9	-0.1	5.0	2.5	-1.2	0.5	6.7
S_{10}	-0.1	5.5	2.75	-0.6	-0.2	7.35

** (-) represents expansion of the measured sample; otherwise dimensional change is registered as shrinkage.*

Cement mortar S_0, whose curve was used for comparison in Fig 1b, exhibits two major dimensional changes. The initial expansion of the sample (0.25 %) can be omitted from the analysis. There is only one notable effect on the dilatometric curve of the cement mortar in the 25 - 230 °C interval. This effect, located at approximately 200 °C, corresponds to the dehydration of free water - capillary pore water, interlayer water and adsorbed water (up to

100 °C), dehydration of gypsum crystal water (100 - 160 °C) as well as dehydration of C-S-H gel. The first significant dimensional change (1.5 %) in cement mortar takes place from 230 to 630 °C (Fig. 1b, Tab. III) and it can be related to portlandite dehydroxylation. The dehydroxylation of $Ca(OH)_2$, usually occurs between 400 and 490 °C. The registered dimensional change in 630 - 900 °C interval is negligible, therefore the line of the diagram can be approximated as constant. Very small expansion (0.1 %) can be attributed to $CaCO_3$ decomposition (normally takes place above 700 °C). The second major shrinkage in S_0 sample takes place above 900 °C due to the sintering process and densification of the given porous material. Even though melting of cement mortar did not take place up to 1200°C, the sample shrunk for 2 % in interval 900 - 1200 °C. Total linear shrinkage of S_0 summed up to 3.65 %.

The samples with fly ash (S_1), zeolite (S_2) and bentonite (S_3) predominantly followed the dimensional change pattern of cement mortar showing two major dimensional changes – one in 230 - 900 °C interval (removal of water from hydrated products, dehydroxylation and decarbonation) and the other one related to the sintering above 900 °C (Fig. 1b; Tab. 3). The first dimensional change in S_1 sample was higher than in cement mortar, summing up to 3.15 %. Also, shrinkage came to abrupt stop at 900 °C in S_1, while the curve line of S_0 proceeded into 'dormant' period from 630 - 1000 °C. This diversity in the behavior points out that the addition of fly ash accelerated the hydration process. Total deformation of the S_1 sample summed up to 4.2 %. The zeolite (S_2) and bentonite (S_3) samples had even more pronounced total changes: 4.6 % and 5.8 %, respectively. The higher dimensional change of S_2 can be attributed to the loss of water located in zeolite cavities and non-framework cations bounded. Dehydration of zeolite takes place from 100 to 200 °C, after which strongly associated water is liberated. The water is completely removed above 500 °C [40]. The changes above 800 °C are related to the rearrangements in the crystalline structure of heulandite [40]. The highest deformation was registered in S_3 mortar. These dimensional changes can be also related to the loss of humidity present in the bentonite addition. Namely, the desorption of hygroscopic water and the loosely bonded water loss takes place between 30 and 210 °C. Dehydration is fully completed up to 600 °C [41]. Also, montmorillonite structure in bentonite swiftly decomposes in short interval upon reaching 850 °C, which can be related to the 2 % shrinkage registered in the S_3 sample during 800 - 900 °C interval (Tab. 3). Thereby the decomposition of heulandite and montmorillonite crystalline structures contributed to the increase in mortar deformation.

The dimensional changes registered in the samples that predominantly comprised zeolite (S_2, S_4, S_5 and S_{10}) were highly influenced its presence (Tab. III). Namely, all of the samples exhibited characteristic changes above 800 °C due to the rearrangements in the heulandite crystalline structure. The shrinkage in 230 – 800 °C and 800 - 900 °C intervals increased with the increase of zeolite content. Thus, S_4 mortar showed initial shrinkage of 2 % which was followed by additional 1 % above 800 °C. S_5 sample exhibited shrinkage of 2.7 % and 1.5 % in mentioned thermal intervals. The addition of bentonite (S_{10}) further increased shrinkage due to the release of bentonite water and subsequent montmorillonite decomposition (5.5 % and 2.75 % changes in 230 - 800 °C and 800 - 900 °C intervals). Total dimensional change for S_4 and S_5 were 3 % and 3.2 % respectively, which is lesser than dimensional change of mortar with fly ash addition (S_1) and solely zeolite addition (S_2) and in range of cement mortar's total shrinkage. The dimensional change of S_{10} sample has the highest shrinkage as it summed up to 7.35 %.

Analogously, the shrinkage of samples with predominant bentonite additive (S_3, S_6, S_7, S_9) was highly influenced by releasing of bentonite water and subsequent montmorillonite decomposition (Tab. III). Bentonite mortars were more prone to thermally induced changes than rest of the observed composites. Also, the increase in bentonite content induced higher shrinkage in 230 - 900 °C interval, as S_6 and S_7 exhibited 4 % and 4.5 % dimensional changes, respectively. The combination of zeolite and bentonite additions influenced further increase in dimensional change. The shrinkage during 230 - 900 °C interval summed up to total 7.5 % in

S_9, while the shrinkage or S_{10} was even higher (8.52 %). Total dimensional change for S_6 and S_7 samples were 4.5 % and 4.6 % respectively, which is higher than dimensional change of mortar with fly ash addition (S_1) and cement mortar, but smaller that of bentonite mortar (S_3). The total shrinkage recorded in three additives sample S_8 summed up to 5.3 %. The dimensional change of S_9 sample has the highest shrinkage by summing up to 6.7 %.

3.2. Physico-mechanical characteristics of the experimental mortars

Workability (W), as rheological characteristic of fresh mortar mixture was decreasing with passing time (0-120 min), only to be stabilized at approximately 60 minutes. The stabilized W value for cement mortar was 135 mm, while for the other mortar mixes this parameter ranged from 95-107 mm. Since w/c ratio was kept constant (0.5) for each mixture, the consistency of the composite mortars was stiffer than that of cement mortar. Since mineral additives require additional amount of water, in the next experiments w/c factor will be applied as variable in order to obtain a satisfactory viscous green mixture. The sample S_1, with fly ash additive, exhibited behavior closest to cement mortar, because spherical fly ash particles helped in packing of cement and sand grains within composite structure. The samples with zeolite addition and fly ash and zeolite combinations produced mixtures with relatively high workability (W_{60min}= 105-113 mm). Bentonite addition gave comparatively dryer mixtures (W_{60min}= 95-97 mm). Bulk density (BD) of green cement mortar was 2290 kg/m^3, while BD of composite mortars ranged from the lowest value for S_3 sample (2000 kg/m^3) to the highest of 2275 kg/m^3 for S_1 mortar. Mortars with zeolite showed approx. 10 % higher bulk density in fresh condition than samples which comprised bentonite.

Experimentally determined physico-mechanical properties (bulk density - BD, shrinkage - SH, water absorption - WA, compressive strength - CS, and flexural strength - FS) of cement mortar and composite mortars were monitored during time period of 28 days. The obtained results after 1, 4, 7, 14, 21, and 28 days were submitted to chemometric analysis, in order to assess the mechanical behavior of mortars during setting and hardening period. The results were correlated to the samples' mix design, i.e. quantity and combinations of applied mineral additives. Upon detecting variations in the results of BD, SH, WA, CS and FS parameters, fitting of the experimental data was conducted using ANN modeling.

3.3. Principal component analysis

Principal component analysis (PCA) applied to the given data set of the results of mechanical properties monitored throughout 28 days, has shown a differentiation between the samples according to variables, i.e. different mineral additives – zeolite (Z), bentonite (B) and fly ash (FA). Subsequently PCA was used as a tool in exploratory data analysis to characterize and differentiate neural network input parameters. The rotation of the principal components was executed by the Varimax method with Kaiser Normalization. The obtained results are condensed in Fig. 2.

As it can be seen in Fig. 2, there is a neat separation of the observed samples according to used assays. Quality results show that the first two principal components, accounting for 93.90 % of the total variability, can be considered sufficient for data representation. Considering the map of the PCA performed on the data, SH, FS and CS exhibited positive scores according to first principal component (each of these variables contributed 27.1-28.3 % of total variance, based on correlations), whereas WA (10.8 % of total variance) showed a negative score values according to first principal component The positive contribution to the second principal component calculation was observed for: WA (51.4 % of total variance, based on correlations) and BD (44.6 %).

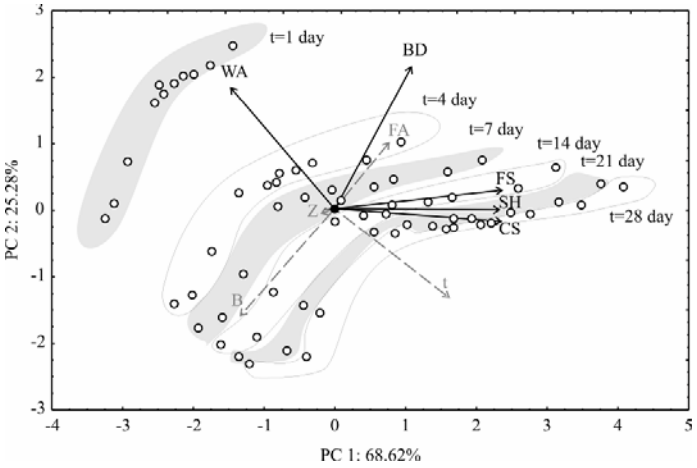

Fig. 2. Biplot graph of physico-mechanical properties experimentally gained for mortars $S_{0\text{-}10}$.

Bulk density (BD), a parameter which can indicate the quality of mortar's mechanical performances, showed the highest values for standard cement mortar during the period of 28 days (BD= 2280-2240 kg/m^3). The sample S_1 with fly ash as additive had somewhat smaller bulk densities (2260-2215 kg/m^3), ranking this composition as the second best. These values were followed by BD for zeolite mortar S_2 (2230-2180 kg/m^3) and bentonite mortar S_3 (1980-1900 kg/m^3). The combination of zeolite and fly ash produced mortars with higher BD (BD_{28}= 2205 kg/m^3 and 2190 kg/m^3 for S_4 and S_5, respectively) than the bentonite and fly ash additive mortar (BD_{28}= 2184 kg/m^3 and 2178 kg/m^3 for S_6 and S_7, respectively). Over-all bentonite addition induced lower values of BD, which ultimately led to lower mechanical strengths. According to BD_{28} values, the combination of zeolite and fly ash as additive gave composite mortars whose density was only 2-3 % smaller than that of cement mortar.

Water absorption (WA) values after 28 days were similar for the fly ash (S_1) and zeolite (S_2) samples: 2.2 % and 2.1 %, respectively. Cement mortar achieved comparatively equal value of water absorption upon hardening (2 %). The bentonite sample (S_3) exhibited even lower WA value: 1.5 %. The elevated water absorption in the fly ash sample can be explained by increased micro-porosity of mortar due to the application of spherical porous ash particles. Bentonite grains are less porous [41] which led to more solidified structure of the composite material. Analogously, the combination of zeolite based additives showed higher WA_{28} in mortar than bentonite additives. Shrinkage (SH) measured on the mortar samples stabilized after 21 days and remained unchanged till the end of hardening period (28 days). The cement mortar showed the highest value of shrinkage (SH_{28}= 0.0812 mm/m) due to the more viscous starting consistency. The S_{28} values of fly ash (S_1), zeolite (S_2) and bentonite (S_3) mortars were as follows: 0.0075 mm/m, 0.053 mm/m, and 0.024 mm/m. Mortars with dryer starting consistency (i.e. bentonite mortars S_3, S_5, S_7) showed smaller shrinkage over time due to lesser quantity of evaporable water in the mixtures.

Mechanical strengths increased over the time, as expected. The initial compressive strength of cement mortar CS_{1day}= 15.4 MP reached the final value of CS_{28day}= 64.6 MPa. Analogously, flexural strength of S_0 increased from starting 5.9 MPa to 11.5 MPa upon hardening. The fly ash sample S_1 showed slightly lower but equally good mechanical strengths: $CS_{1\text{-}28day}$= 14.8 -61.4 MPa and $FS_{1\text{-}28\ day}$ = 5.5 -10.4 MPa. Final strengths for zeolite (S_2) and bentonite (S_3) mortar were: CS_{28day} = 45.7 MPa / FS_{28day}= 8.0 MPa and CS_{28day} = 21.3 MPa/FS_{28day} = 5.0 MPa. The combination of fly ash and zeolite in ratio 2:1 produced higher strengths than the sample that included higher share of zeolite in the combined additive. The difference between their final strengths was approximately 15 %. The same correlation appeared in bentonite-fly ash samples, i.e. the difference in final strengths was 17 %. The

lowest values of mechanical strengths were obtained for S_3, meaning that bentonite particles created less porous mortar structure but their adhesion on sand grains was not successful which did not result in a strong cementing bond.

The differentiation among samples prepared with different additives is evident on the PCA graphic. Namely, the fly ash and zeolite samples with the highest FS, SH and CS values were observed in the right side of the PCA plot. The process time coordinate is positively correlated to FS, SH and CS and negatively related to WA. The highest WA values (i.e. fly ash sample) are noticed to the upper left of the PCA graph. The content of fly ash is positively correlated to BD, FS and CS, while the correlation between these parameters and bentonite (B) is negative. The content of zeolite (Z) is less influential on BD, FS and CS that fly ash (FA) according to PCA. Also, according to the results SH, CS and FS are bonded in a strong positive correlation. These variables are also negatively correlated with WA. BD is positively correlated to SH, CS and FS, and also positively correlated to WA.

3.4. Response Surface Methodology

The second order polynomial models for all observed variables were found to be statistically significant and the response surfaces were fitted to these models.

According to ANOVA (Tab. IV), the linear term of bentonite (B) content were the most influential for SH, CS, FS and BD calculation, as well as the linear term of time (*t*) in SOP model, statistically significant, at $p<0.01$ level. The linear term and the quadratic term of *t* were the most influential for WA calculation ($p<0.01$ level). The quadratic terms of *t* were very influential terms in SOP models for SH, CS, FS and BD calculation ($p<0.01$ level). All SOP models had an insignificant lack of fit tests, which means that all the models represented the data satisfactorily. The coefficients of determination for response variables were relatively high, showing the good fit capability to represent the experimental results.

Tab. IV ANOVA calculation of developed SOP models.

	df	SH	WA	CS	FS	BD	W		SH	WA	CS	FS	BD	W
FA	1	0.000^{*}	0.5	36.3^{**}	0.478^{**}	1727.4	5.1	χ^2	0.000	2.418	8.843	0.135	759.19	15.63
FA²	1	0.000^{*}	0.5	36.0^{**}	0.487^{**}	2304.0	5.8	**RMSE**	0.006	1.483	2.835	0.350	26.27	3.732
Z	1	0.000^{*}	0.5	38.4^{**}	0.518^{**}	1756.2	5.1	**MBE**	0.000	0.000	0.000	0.000	0.000	0.000
Z²	1	0.000^{*}	0.5	36.4^{**}	0.454^{**}	1279.7	5.3	**MPE**	17.105	35.831	9.214	4.642	0.900	2.575
B	1	0.007^{+}	6.9	2656.0^{+}	79.586^{+}	314121.1^{+}	4771.5^{+}	r^2	0.922	0.804	0.964	0.967	0.948	0.924
B²	1	0.000^{*}	0.5	37.6^{**}	0.483^{**}	1565.1	5.5	**adj. r²**	0.905	0.760	0.955	0.960	0.936	0.936
t	1	0.001^{+}	64.1^{+}	710.3^{+}	4.400^{+}	6757.8^{+}	19.9	**Skew**	0.132	-0.055	0.019	-0.143	0.060	0.172
t²	1	0.002^{+}	164.7^{+}	368.3^{+}	12.791^{+}	2531.1^{**}	425.6^{+}	**Kurt**	0.458	-1.299	-0.119	-0.722	0.513	0.403
FA×Z	1	0.000^{*}	0.5	35.6^{**}	0.459^{**}	1678.3	6.1	**Mean**	0.000	0.000	0.000	0.000	0.000	0.000
FA×t	1	0.000	0.1	2.2	0.420	0.0	29.4	**StDev**	0.006	1.494	2.857	0.353	26.47	3.766
Z×t	1	0.000	0.1	121.6^{+}	2.696^{+}	310.4	150.1	**Var**	0.000	2.232	8.162	0.125	700.79	14.18
B×t	1	0.000^{+}	0.7	564.5^{+}	6.805^{+}	964.5	182.4^{+}							
Error	53	0.002	145.1	530.6	8.097	45551.2	766.0^{+}							

$^{+}$Significant at $p<0.01$ level, *Significant at $p<0.05$, **Significant at $p<0.10$ level.

A three-dimensional graphics of the response variables were plotted for the comparison with experiment data visualization (Fig. 3).

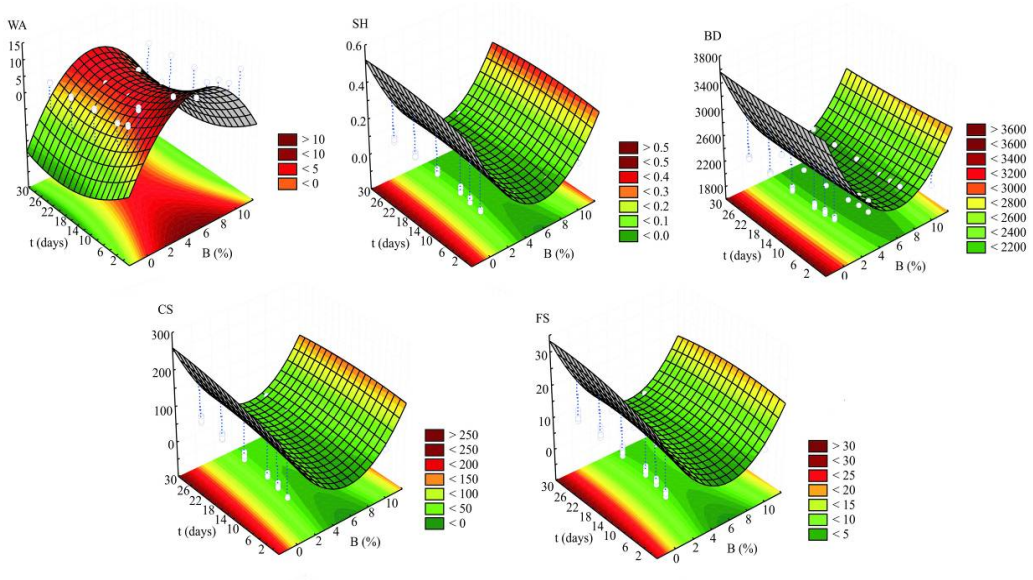

Fig. 3. Visualization of the response variables determined by SOP model.

The coefficients of determination (r^2) for SOP models were rather good (0.804–0.967). The quality of the model fit was tested (Tab. IV), the higher r^2 values, and the lower χ^2, MBE, RMSE and MPE values show the better fit to the experimental results. The residual analysis of the developed model was also performed. Skewness measures the deviation of the distribution from normal symmetry. If the skewness is clearly different from zero, then the distribution is asymmetrical, while normal distributions are perfectly symmetrical. Kurtosis measures the "peakedness" of a distribution. If the Kurtosis is clearly different than zero, then the distribution is either flatter or more peaked than normal; the Kurtosis of the normal distribution is zero. The average, the standard deviation (SD), the standard error (SE) and the variance of residuals have also been analyzed and shown in Tab. IV.

The residual analysis showed that the mean of residuals were equal to zero, and the standard deviation was 0.006 - 26.472. These results showed a good approximation to a normal distribution around zero with a probability of 95 % (2×SD), which means a good generalization ability of the developed model for the range of observed experimental data.

3.5. Neurons in the ANN hidden layer

All variables considered in the PCA and RSM calculations, were also used for the ANN modeling. ANN modeling was performed for prediction of SH, WA, CS, FS and BD. Determination of the appropriate number of hidden layers and the number of hidden neurons in each layer is one of the most critical tasks in ANN design. The number of neurons in a hidden layer depends on the complexity of the relationship between inputs and outputs. The optimum number of hidden neurons was chosen upon minimizing the difference between predicted ANN values and desired outputs, using Sum of Squares (SOS) during testing as a performance indicator. According to the results, it was noticed that the optimal number of neurons in the hidden layer for SH, WA, CS, FS and BD calculation was 4. The quality of the model fit was tested of the developed model was presented in Tab. V. The used training algorithm was BFGS 71, and the activation functions were logistic and exponential (for hidden and output layer, respectively).

Tab. V Performance of the optimal ANN (Network name: MLP 4-4-5).

	SH	WA	BD	CS	FS	Error
Training	0.980	0.994	0.990	0.993	0.990	0.004
Testing	0.976	0.991	0.988	0.986	0.994	0.010
Validation	0.944	0.980	0.979	0.964	0.986	0.014

3.6. Sensitivity analysis

The influence of the input over the output variables, i.e. calculated changes of the output variables for infinitesimal changes in the input variables are shown in Fig. 4.

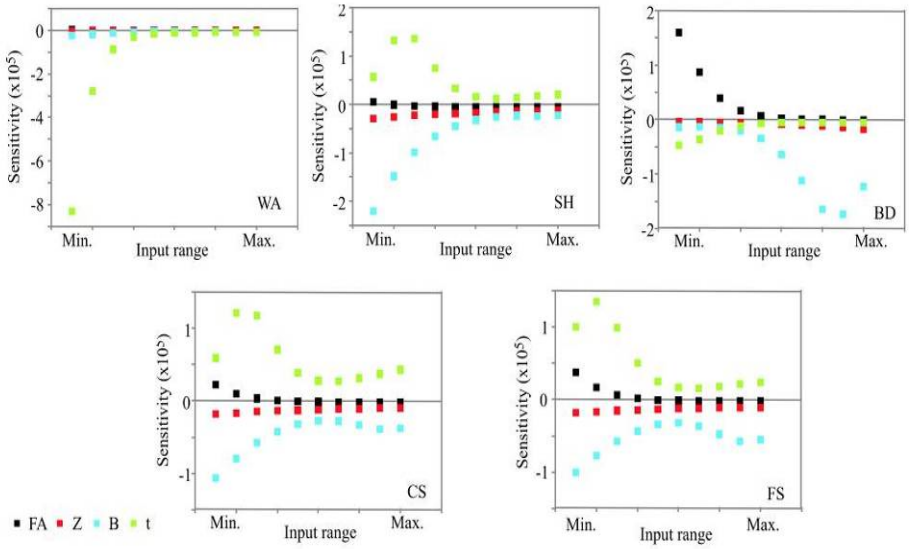

Fig. 4. Sensitivity analysis - the influence of the input over the output variables.

As it can be seen in Fig. 4, SH, WA, CS, FS and BD were most affected by the infinitesimal changes in time (*t*) at the minimum values of the input space (1 day). The influence of *t* is diminished afterwards. The effect of the infinitesimal changes in B content on SH, CS and FS, was most influential close to the minimum of the input space. BD was most affected by the infinitesimal changes of B content at the maximum of the input space. The influence of FA addition is also observed in CS, FS and BD, where the highest impact is observed in the minimum of the input space. Therefore, analytical modeling confirmed that fly ash-zeolite mortars exhibit mechanical behavior closest to standard cement mortar, while the most significant diversities were observed in samples that included bentonite additive.

3.7. Microstructural analysis of experimental mortars

Cement mortar and experimental mortars were analyzed via scanning electron microscope. The results are illustrated in Fig. V (a-f).

The microstructure of each of the cementitious composites was composed of a grain mixture - cement, sand and mineral additives. The particle sizes in the recorded areas significantly varied between 1 μm and cca 30 μm. The surface of each sample comprised multitude of pores and micro-cavities. Cementing matrix (Fig. 5 a-f), merged together coarser sand particles. The matrix is composed of number of mineral phases that are predominantly related to minerals developed during hydration. As hydration proceeds, formerly clear surface of cement particle is being covered with

unbound debris. The new formations are hydration products such as tricalcium aluminate, brownmillerite, portlandite and calcite. The coating of "lumps and platelets" is being created on the top of the particle, while unhydrated part remains beneath it [44, 45]. Upon conducted hydration, thus formed layer of cement minerals is merged together with sand particles creating a solid composite structure.

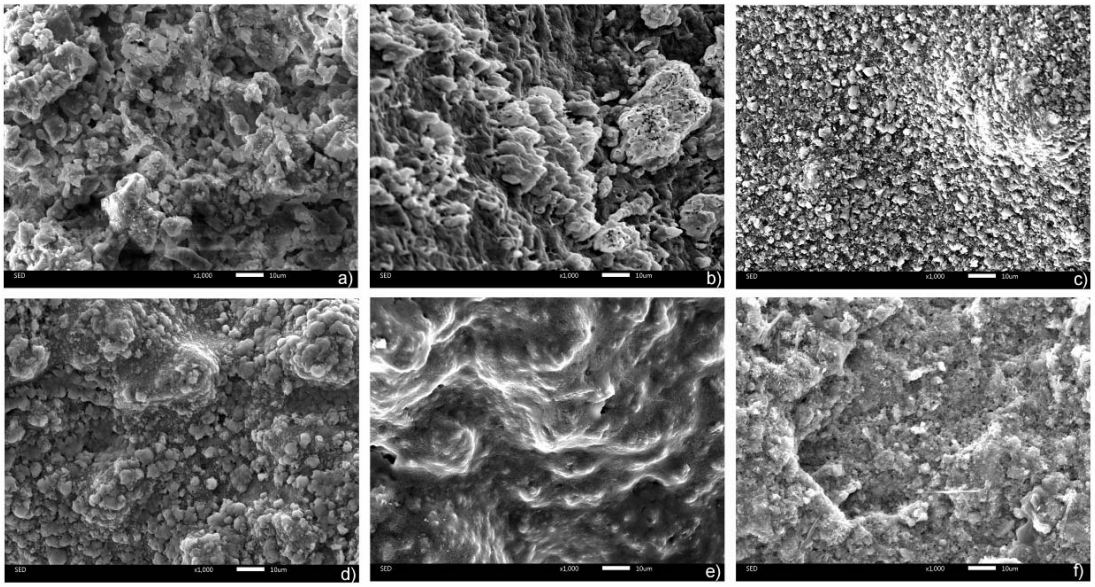

Fig. 5. SEM microphotographs of a) S_0, b) S_1; c) S_2, d) S_3; s) S_4 and f) S_6 mortars.

The microstructure of standard cement mortar (S_0) upon completed hardening (Fig. Va) consists of sand grains (20-30 μm) bonded and covered by hydration products debris, i.e. cement mineral particles sizing up to 10 μm. The cement particles are closely integrated with the sand grains. Very small crystals within the mixture correspond to calcite. Coarser crystals are sparite and microcrystalline ooid formations are micrite (0.06-4 μm). Microcrystalline prisms and six-sided pyramids correspond to quartz. Furthermore, ettringite is recognized as rod-shaped particles and carboaluminates appear as needles and laths [44, 45]. The pores are regularly shaped and round with diameter varying from 2 to 10 μm, without visible interconnections and channel formations. The S_1 mortar (Fig. 5b) showed comparatively denser microstructure due to the application of fly ash additive, which eased "packing" and left less voids between cement and sand grains. The visible mixture comprises predominantly spherical and hollow particles, and certain amount of irregularly shaped crystalline formations. The particles with increased superficial micro-porosity and pore diameter smaller than 1 μm correspond to fly ash. The overall porosity is smaller than in S_0, while the average pore is 2-3 μm. The S_2 mortar exhibited nodular and small-grained structure, as it can be seen in Fig. Vc. The hydration products crystals are smaller than in S_0 and S_1. Besides the products of the cement hydration, tabular and/or parallel crystals characteristic for zeolite mineral heulandite are present within the surface debris. Pores are evenly, but more frequently distributed on the surface of the mortar. Average pore is round with very small diameter (1-2 μm). S_3 mortar (Fig. 5d) also showed a fine grained structure, however the crystalline formations were comparatively coarser than in S2. Also, the level of visible porosity is lower. Agglomerations and clusters that formed on the surface comprised bentonite mineral phases, besides usual cement minerals particles. Namely, montmorillonite appeared as stacks of rectangular platelets merged with irregularly shaped massive quartz crystals. The combination of fly ash and zeolite as mineral additive used in the S_4 mortar produced a very dense

structure with only few scattered pores (Fig. 5e). The size of the pores was, however, comparatively bigger (approx. 5 μm) that in other mortars. The stiffer consistency of S_6 mortar led to more porous structure of the mortar upon hardening (Fig. 5f). The average pore size in S6 was less than 1 μm (approx. 0.5 μm).The microstructural analysis suggests that zeolite and fly ash combination as mineral additive produced a favorable structure able to provide good mechanical properties, which is in accordance with mathematical models and experimental results.

4. Conclusion

Fly ash and sorptive clays were incorporated in the design of mortar as a novel solution for an ecological material with good performances and ability to prevent heavy metals from leaching into environment by immobilize them in clay structure. Thermo-mechanical behavior of ten mortars with different combinations of minerals additives was monitored. The main conclusions are summarized below:

- The formation of molten phase in mortars was not observed up to1200 ^{o}C);
- Addition of zeolite and bentonite did not interfere with the cement hydration route, as DTA curves of composite mortars showed only minor differences to standard cement mortar.
- Bentonite mortars were more prone to thermally induced changes than rest of the observed composites, having higher dimensional change. Dimensional change of zeolite mortars was in range of cement mortar shrinkage.
- The combination of fly ash and zeolite in ratio 2:1 produced the highest mechanical strengths. The lowest strength values were obtained for mortar with solely bentonite addition.
- The ANN model showed high prediction accuracy (r^2 = 0.989). Analytical modeling confirmed that fly ash-zeolite mortars exhibit behavior closest to standard cement mortar, while the most significant diversities were observed in samples that included bentonite additive.

Acknowledgments

This investigation was supported by Ministry of Education, Science and Technological Development of the Republic of Serbia, and conducted under Projects: III 45008 and ON 172057. The authors would like to express mutual gratitude to dr Smilja Marković (Institute of Technical Sciencies of SASA,Serbia) for providing help regarding the thermal analysis and to dr Aleksandra Milosavljević and dr Ana Kostov (Mining and Metallurgy Institute Bor, Serbia) for performing SEM recording.

5. References

1. K. Samimi, Constr. Build. Mater. 151 (2017) 292.
2. A. Ramezanianpour, Constr. Build. Mater. 101 (2015) 347.
3. I. Yuksel, T. Bilir, O. Ozkan, Build. Environ. 42 (2007) 2651.
4. H. Chu, J. Jiang, W. Sun, M. Zhang, Constr. Build. Mater. 153 (2017) 682.
5. T. Alomayri, Ceram. Inter. 43:5 (2017) 4576.
6. A. Terzić, L. Pezo, V. Mitić, Z. Radojević, Ceram. Inter. 41: 2 (2015) 2714.
7. R. Silva, P.Guetti, M. Luz, F. Rouxinol, R.Gelamo, Build. Mater. 149 (2017) 378.
8. V. Karayannis, A. Moutsatsou, E. Katsika, Sci. Sinter. 48 (2016) 363.
9. S. Y. Choi, Y. S. Choi, E. I.Yang, Constr. Build. Mater. 165 (2018) 424.
10. D. Nagrockiene, G. Girskas, Constr. Build. Mater. 113 (2016) 964.

11. S. Afzal, K.Shahzada, M.Fahad, S.Saeed, M.Ashraf, Const. Build. Mater. 66 (2014) 403.
12. S. Aydın, B. Baradan, Cement Concr. Res. 37 (2007) 988.
13. A. Terzić, Lj. Pavlović, Lj. Miličić, J. Coal Prep. Utiliz. 33:4 (2013) 159.
14. P. Heede, M. Keersmaecker, A.Elia, A.Adriaens, N.Belie, Cement Concr. Compos. 80 (2017) 210.
15. M. Nadesan, P. Dinakar, Case Studies in Construction Materials 7 (2017) 336.
16. R. Kurda, J. Brito, J. Silvestre, Cement Concr. Compos. 84 (2017) 198.
17. K. Zabielska-Adamska, J. Hazard. Mater. 151: 2–3 (2008) 481.
18. K. Kawai, Constr. Build. Mater., 67 (2014) 55.
19. C. Belviso, F. Cavalcante, S. Gennaro, A. Palma, S. Fiore, Fuel 144 (2015) 369.
20. N. Gupta, V. Gedam, C. Moghe, P. Labhasetwar, Environ.Technol.Innovation, 7 (2017) 152.
21. E. Vejmelkova, D. Konakova, T. Kulovana, Cement Concrete Comp. 55 (2015) 259.
22. M. Najimi, J. Sobhani, B. Ahmadi, M. Shekarchi, Constr. Build. Mat. 35 (2012) 1023.
23. D. Nagrockiene, G. Girskas, Constr. Build. Mater. 113 (2016) 964.
24. S. Andrejkovicova, C.Alves, A.Velosa, F.Rocha, Cement Concr. Compos. 60 (2015) 99.
25. C.Colella, W.Wise, The IZA Handbook of Natural Zeolites, Micropor. Mesopor Mat. 189(2014)4.
26. R. Malekian, J. Abedi-Koupai, S. Eslamian, et al., Appl. Clay Sci. 51 (2011) 323.
27. E. Uzunova, H. Mikosch, J. Hafner, J. Mol. Struc.: THEOCHEM 912 (2009) 88.
28. L. Hortigüela, A. Pinar, J. Pariente, et al, Micropor. Mesopor. Mat. 193 (2014) 93.
29. L. Zhirong, A. Uddin, S. Zhanxue, Acta Part A 79 (2011) 1013.
30. E. Ayuso, A. Sanchez, Clay Clay Miner. 51 (2003) 475.
31. S. Afzal, Constr. Build. Mater. 66 (2014) 403.
32. S. A. Memon, Constr. Build. Mater. 30 (2012) 237.
33. T. Shojaeimehr, F. Rahimpour, M. Khadivi, M. Sadeghi, J. Indust. Engin. Chem. 20 (2014) 870.
34. A. Hosseini, M. Ahmadi, M. Ghiasvand, A. Tardast, R. Katal, J. Industrial.Eng. Chem. 19 (2013) 1044.
35. M. Moliner, J. Serra,A. Corma,E. Argente, S. Valero,V. Botti, Micropor. Mesopor. Mater. 78 (2005) 73.
36. N. Hilal, O.Ogunbiyi, M. Al-Abri, Desalination, 228:1–3 (2008) 175.
37. M. Tatlier, H. Cigizoglu, A.Senatalar, Computers & Chemistry, 26 (2002) 557.
38. H. Abdi, L. Williams, Principal component analysis, Computational Statistics, 2 (2010) 433.
39. B. Taylor, Methods and Procedures for the Verification and Validation of Artificial Neural Networks (2006), Springer, USA, ISBN-13: 978-0-387-28288-6.
40. A. Terzić, L. Pezo, Lj. Andrić, Compos. B 109 (2017) 30.
41. S. Pandey, V. Buljak, I. Balac, Sci. Sinter. 49 (2017) 331.
42. E. Qoku, T. Bier, T. Westphal, J. Build. Engin., 12 (2017) 37.
43. P. Claisse, Introduction to cement and concrete, Civil Engin. Mater., (2016) 155.
44. A. Parra, M. Vlasova, P. Aguilar, T. Tomila, Sci. Sinter., 49 (2017) 207.
45. I. Galan, H. Beltagui, M. Mate, F. Glasser, Cem Concr Res 84 (2016) 85.

Садржај: *Минерални додаци се често употребљавају као замена за цемент како у конструкционим бетонима тако и у малтерима. Летећи пепео је један од најчешће примењиваних додатака који унапређује реолошка својства, као и термичке и механичке карактеристике малтера, и као такав је опсежно истраживан. Овај индустријски нуспродукат садржи тешке метале у свом саставу због чега је неопходно оптимизовати његову дозажу при дизајну малтера. Међутим, постоје глине са сорптивним својстима, као што су природни зеолит и бентонит, које могу да предупреде миграцију токсичних елемената из пепела имобилишући их у својој структури. Десет експерименталних малтера је припремљено на бази Портланд цемента, речног песка и додатака – летећег пепела, зеолита и/или бентонита у складу са правилима хемометријског експерименталонг дизајна. Циљ рада је био да се испита утицај минералних додатака на термичка и механичка својства малтера. Термичка својства су праћена методама дилатомерије и DTA анализе. Метода главних компонената (ПЦА) је примењена при анализи резултата физичко-механичких испитивања (обрадљивост, запреминска маса, скупљање, притисна и савојна чврстоћа) како би се узорци разврстали у факторном простору. Перформансе вештачких неуронских мрежа упоређене су са експерименталним резултатима у циљу добијања брзог и превизног модела за предикцију механичких параметара малтера. АНН модел је показао високу тачност у предвиђању (r^2 = 0.989). Резултати истраживања су указали да се применом ових минералних додатака можу добити економични малтери са довољно добрим перформансама. Међутим, алатке аналитичког моделовања су издвојиле малтер са додатком летећег пепела и зеолита као материјал са најоптималнијим механичким својствима.*

Кључне речи*: дилатометрија, DTA; аналитичко моделовање; SEM; конструкциони композити.*